Materials Research Express

PAPER • OPEN ACCESS

Cu based Metal Organic Framework (Cu-MOF) for electrocatalytic hydrogen evolution reaction

To cite this article: Ravi Nivetha *et al* 2020 *Mater. Res. Express* **7** 114001

Materials Research Express

PAPER

Cu based Metal Organic Framework (Cu-MOF) for electrocatalytic hydrogen evolution reaction

Ravi Nivetha[1], **Aparna Sajeev**[1], **Aleena Mary Paul**[1], **Kannan Gothandapani**[1], **Subashini Gnanasekar**[1], **George Jacob**[1], **Raja Sellappan**[1], **Vimala Raghavan**[1], **Krishna Chandar N**[3], **Sudhagar Pitchaimuthu**[4], **Soon Kwan Jeong**[2] **and Andrews Nirmala Grace**[1]

[1] Centre for Nanotechnology Research, Vellore Institute of Technology, Vellore, Tamil Nadu-632014, India
[2] Climate Change Technology Research Division, Korea Institute of Energy Research, Yuseong-gu, Daejeon, 305-343, Republic of Korea
[3] Department of Physics, School of Advanced Sciences, VIT University, Vellore, India
[4] Photocatalyst and Coatings Group, SPECIFIC, College of Engineering, Swansea University (Bay Campus), Fabianway, Swansea, United Kingdom

E-mail: anirmalagladys@gmail.com

Keywords: hydrogen evolution reaction, copper, 1, 3, 5 benzene tricarboxylic acid, hydrogen evolutio metal organic frameworks (MOFs)

Supplementary material for this article is available online

OPEN ACCESS

RECEIVED
10 June 2020

REVISED
12 August 2020

ACCEPTED FOR PUBLICATION
18 August 2020

PUBLISHED
18 November 2020

Abstract

Hydrogen production using novel catalysts is regarded as one of the most needed technology for the future economic needs and water splitting to give H_2 gas, which is a challenging task for large-scale production. This work reports the synthesis of Meso-Cu-BTC metal organic framework and further used for understanding its role in electrochemical hydrogen evolution reaction (HER) in 1 M NaOH solution. Meso-Cu-BTC electrocatalyst showed a less overpotential of 89.32 mV and an onset potential of 25 mV with an appreciable current density. Results show a low Tafel slope of 33.41 $mVdec^{-1}$ and long-term durability. Thus, the overall results show that Meso-Cu-BTC acted as a good candidate for electrocatalysis towards hydrogen evolution.

1. Introduction

With an increase in population and industrialization, there is huge energy demand. Use of fossil fuels creates many issues like environmental pollution, anthropogenic CO_2 emission leading to climatic change and global warming [1–3]. To avoid these issues, hydrogen fuel is the only way to replace the burning hydrocarbon fuels and an eco-friendly source of energy towards building clean and sustainable energy technology [4, 5]. Hydrogen economy will require an efficient and sustainable H_2 production method. However, challenges to produce hydrogen in large scale and its storage have its obstacles in the application towards renewable energy [6, 7]. Currently water splitting process via electrochemical and photoelectrochemical are effective methods to produce large-scale hydrogen energy with zero emission of carbon [8, 9]. These are advantageous of sustainable energy source, but the other and main critical requirement is a catalyst. Among the various methods, electrolysis water splitting is the simplest route to produce large scale H_2 from water and is extensively been investigated as a promising conversion system. Electrochemical water splitting is a source to harness renewable energy to produce H_2. However a substantial overpotential is needed to overcome the huge energy barrier to drive hydrogen evolution, which is a high energy process and hence an efficient electrocatalyst is desirable to reduce the activation. The electrochemical water splitting is generally investigated in two types of electrolytes such as alkaline and acid medium; numerous electrocatalyst has been tested in acidic medium for HER. Research has been shifting towards the alkaline environment to reduce the effects of corrosion and allowing an extension of the choice of electrode materials. An efficient electrocatalyst possessing superior catalytic properties for hydrogen evolution reaction should have less overpotential, stability with a low Tafel slope. Pt and Pt group metals are mostly investigated as electrocatalysts towards HER, due to its near-zero onset potential, high activity, low overpotential and excellent stability but its usage is limited for hydrogen production because of its high cost and scarcity. Hence a catalyst alternative to Pt is essential to produce cost-effectiveness and high-performance

electrocatalytic activity for HER. Non-metallic catalysts include transition metal phosphides, metal sulfides and its alloys [10–14]. For instance, Vikraman *et al* demonstrated heterostructured MoS_2-WS_2 electrocatalyst for HER activity in acid medium. Results displayed that it follows Heyrovsky mechanism at an overpotential of 120 mV with Tafel slope being 72 $mVdec^{-1}$ [15]. Fulong Wang *et al* described FeP as a good catalyst showing excellent durability in basic medium and a good catalyst for electrolysis. It was observed that the HER activity of FeP powder showed a Tafel slope of 93 $mVdec^{-1}$, overpotential of 24 mV and controlled by Volmer reaction [16]. Liang Ma and group demonstrated that Mo_2C and Mo_2N are efficient catalysts for electrochemical hydrogen evolution with 100 $mVdec^{-1}$ Tafel slope, an overpotential of 353 mV for the nitride whereas, for Mo_2C, 56 $mVdec^{-1}$ was observed with an overpotential of 293 mV respectively. Hence the results exhibit that Mo_2C is more electrochemically active than Mo_2N towards hydrogen evolution reaction. Though the above-said catalysts showed good performance, there is yet a lot of space to synthesize cost effective catalysts without compromising on the performance for hydrogen evolution reaction towards commercial systems. Porous class materials have attractive applications in energy both for storage and conversion. A very recent material of interest are the metal organic frameworks also abbreviated as MOFs, which are porous based materials and the same are synthesized, designed by assembling organic ligands and metal nodes, wherein the organic ligands come from the ligand linkers used during the synthesis. Metal organic framework (MOF) is an interesting class of porous crystalline compounds and is an organic-inorganic hybrid material [15–17]. MOFs are known for its unique structural features like porous nature, large specific surface area with tunable pores. MOF materials are ions or cationic metal oxo clusters, which are coordinated with anionic organic linkers especially carboxylates or phosphonates, but also imidazolate ions and sulfonates due to its inherent structural properties such as uniformity but tunable cavities, attracting optical, electrical, physiochemical properties with tailorable chemistry and large surface area. MOFs have been used for a variety of applications viz. separation of gases, gas sensing, optical devices, photocatalytic degradation, biomimetic applications, magnetism and organic molecule adsorption [18–24]. Recently, MOFs are exploited for H_2 fuels and have also been utilized as HER electrocatalysts via electrochemical water splitting. Qin and group developed POM based MOF for HER activity [25]. 2D ordered MOF film with cobalt dithiolene catalytic centres achieved high catalytic efficiency for HER under acidic medium [26]. Around 20,000 metal organic frameworks are known to date and amongst it, the class of HKUST-1 or Cu-BTC compounds was reported by Chuiand group [24]. Cu-BTC is a paddle-wheel shaped structure with Cu metal corners linked by benzene 1,3,5-tricarboxylate organic linkers. In Cu-BTC structure, two Cu atoms are found in each metal corners, which are further bonded to the four oxygen atoms from BTC linker with a formation of four connected square-planar vertexes and another axial coordination sites are regarded as open metal sites [27–29]. Copper-based MOFs and derived porous carbon catalyst is easy to synthesize. It has numerous properties such as high chemical stability, redox activity, electro and photochemical properties and biocompatibility and widely investigated with diverse applications such as photovoltaics, hydrogen storage, ammonia sensing, absorption, HER and CO_2 reduction [30–34]. For instance, Jahan-Bakhsh Raoof *et al* developed the MOF derived nanoporous carbon/Cu as an electro-catalysts for HER in acid medium, which exhibited a Tafel slope of 34.0 mV per decade with an exchange current density of 1.2 $mAcm^{-2}$ [35]. Sakineh Mandegarzad and group demonstrated the use of Cu-Pd bimetallic nanoparticle supported nanoporous carbon composite as electrocatalyst towards HER in acid medium. Results showed 200 mV as overpotential with 28.2 $Vdec^{-1}$ as Tafel slope [36]. Ting Song *et al* demonstrated copper (II) organic framework with high stability towards improved visible light photocatalysis towards hydrogen evolution. Results show that the Cu based MOF produces maximum hydrogen evolution rate (5.7 $mmolh^{-1}$) along with long-term stability under visible light irradiation [37]. Herein, a simple route was used for the facile synthesis of Meso-Cu-BTC MOF and was further used as electrocatalyst towards the outstanding performance of HER in alkaline medium. As a result, the catalysts showed a low overpotential 89.32 mV, onset potential (25 mV), low Tafel slope (33.41 $mVdec^{-1}$) with a high current density and long-term durability.

2. Experimental section

2.1. Materials

The chemicals and reagents used in this work are of analytical grade and used as received without the need for any further purification. Copper nitrate hemipentahydrate ($Cu(NO_3)_2.2.5H_2O$), benzene 1,3,5 tricarboxylic acid (H_3BTC), N, N Dimethylformamide (DMF), ethanol, dichloromethane were procured from Sigma-Aldrich and deionized water was used in the preparation.

2.2. Preparation of Meso-Cu-BTC

Meso Cu-BTC was synthesized under solvothermal conditions as per the literature report with a slight modification [38]. Typically, 24 mmol of benzene 1,3,5 tricarboxylic acid, 43 mmol copper (II) nitrate

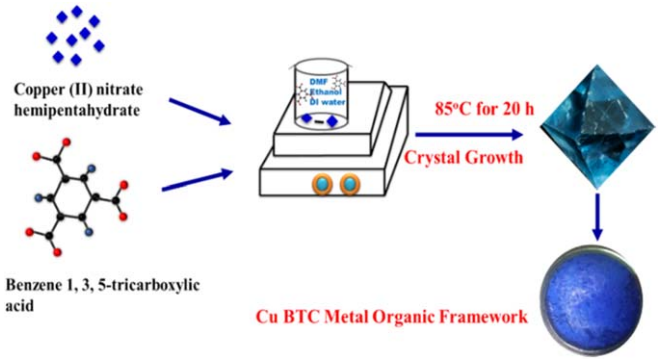

Scheme 1. A Schematic diagram of preparation of Cu-BTC Metal organic Framework.

hemipentahydrate were dissolved in 250 ml solvents consisting equal ratio of N, N dimethylformamide, ethanol and deionized water respectively. The reactant was further agitated for 15 min under ambient conditions and the mixture was further transferred, heated in an oven at 85 °C for 20 h. Later it was thoroughly washed with DMF and then kept in dichloromethane (50 ml) for 3 continuous days and exchanged once every 12 h to finally get the blue coloured Meso-Cu-BTC MOF crystals, which was dried at 170 °C under vacuum for 8 h. A schematic of the preparation Meso-Cu-BTC is given in scheme 1.

2.3. Material characterization

Powder x-ray diffraction pattern was obtained with a Rigaku Miniflex x-ray diffractometer with Cu Kα (1.5406 Å) 2θ range from (5° to 60°). Functional group analyses were done by FTIR - (Shimadzu Affinity-1). To understand the thermal stability of the sample, the experiments were maintained under N_2 at a rate of 5 °C min^{-1} with a SDT Q600 (TGA Instruments, Korea). The samples were heated from ambient temperature to 500 °C. N_2 adsorption/desorption BET isotherms were obtained using a Micrometrics ASAP 2020 analyser at 196 °C. Further the surface area was calculated using Brunauer–Emmett–Teller method. The degassing was done at 180 °C overnight under vacuum before the measurement. The surface morphology was analysed by FE-SEM, model-Hitachi SU6600. Raman measurements were done by the Horiba Olympus plus with 532 nm green laser.

2.4. Electrochemical details

Electrochemical hydrogen evolution was performed by a traditional three electrode probe in a CHI-660C instrument. The GCE was used as a working electrode with geometric surface area being 0.071 cm^2 and polished with 0.05 micron alumina, rinsed with double distilled water, further sonicated in ethanol and water for its activation, which was further dried at room temperature. Before the experiments, the electrodes were electrochemically subjected to several cycling from 0.1 to 0.4 V versus Ag/AgCl. Meso-Cu-BTC slurry catalyst was then drop casted onto the well-cleaned GCE, which was further dried at ambient temperature for 12 h. As a reference, the electrocatalytic activity of commercial Pt electrode was evaluated under the same testing conditions. All the potentials were measured with respect to RHE (reversible hydrogen electrode) as per the below equation

$$E_{vs.}RHE = E_{vs.}(Ag/AgCl) + 0.059.pH + 0.199(V)$$

Linear sweep voltammetry (LSV) was recorded in the electrolyte solution and from the same, Tafel slopes were calculated. To further understand the stability, the same was evaluated by the polarization test.

3. Results and discussion

3.1. Structure, morphological analysis of the catalyst

The well crystalline nature of Meso-Cu-BTC octahedral crystals was further confirmed using XRD measurements [39] and the same is given in figure 1. Results confirmed that the experimental XRD pattern is congruous with those reported in the literature [40], which revealed that the solvothermal conditions has rendered a good crystalline phase and no other phase crystallinity could be detected. Thus, the XRD results confirm that a pure Meso-Cu-BTC phase is formed. In the spectrum, the main diffraction peaks were seen at 6.6°, 9.44°, 11.76°, 13.71°, 15.14°, 16.73° and 19.23°, which could be assigned to (200), (220), (222), (400), (331) and (440) crystalline planes of MOF. The highest intense peak was observed at 11.76°, which referred to a high

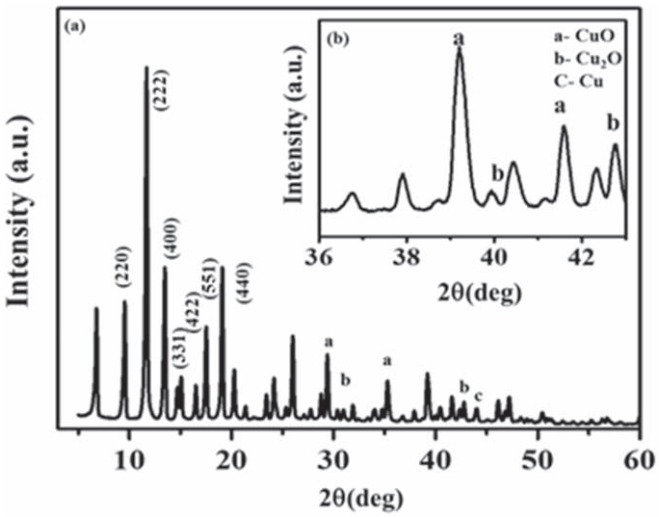

Figure 1. X-ray diffraction pattern of Cu-BTC metal organic framework (inset shows the expanded view).

degree of crystallinity. Some low intense weak peaks are observed in the range of 35.4° to 43.0°, which indicates a minor presence of Cu_2O phase (inset of the figure 1(a)). Reports suggest that high temperature could produce Cu_2O during the formation of Meso-Cu-BTC MOFs [41, 42]. The morphology and the textural structure was further analyzed by FE-SEM, optical analysis and the same is given in figure 2 and figure 3. As could be seen from the images, the prepared MOF possessed cubic crystals with octahedral geometry with the length of each octahedral edge around 10–20 μm [43]. The EDX spectrum was further used to confirm the element present in Meso-Cu-BTC MOF (figure 2(d)), which revealed the presence of Cu and O further confirming the formation of Cu-BTC in accordance with the literature [44].

3.2. Elemental and surface analysis

FT-IR is a useful tool to understand the functional groups and analyze the molecular structure of Meso-Cu-BTC MOF [45]. Figure 4 shows the band at 480 and 720 cm^{-1} attributed to the bending and stretching vibrational modes of Cu–O [46]. The minor peaks between 660–760 cm^{-1} are due to the bending vibration in and out plane of the aromatic ring. The bands from 800–1150 cm^{-1} are due to the symmetric and asymmetric modes of O–C=O and C–O stretching vibrations of moieties. Further, the strong absorption bands are assigned at 1375, 1432 and 1625 cm^{-1}, which could be due to the vibrations of carboxylate group of Meso-Cu-BTC. These are similar to the asymmetric, symmetric types of C=O and stretching mode of C–O respectively due to the binding of carboxylate (COOH groups) with Cu ions [47, 48]. The band at 1542 cm^{-1} is due to water coordinated within the Cu-MOF framework. The peak at 3309 cm^{-1} is due to the surface adsorbed water and OH group in the Meso-Cu-BTC framework and the peak at 1719 cm^{-1} is due to benzene tricarboxylic acid in the catalyst thereby proving the formation of Meso-Cu-BTC framework. Raman spectrum is an advanced analytical technique to identify the organic bonding of Meso-Cu-BTC MOF to give further insights about the framework structure (figure 5). As seen in the spectrum, the peaks till 600 cm^{-1} is due to vibrational modes involving Cu^{2+} ions. The peaks from 200 to 270 cm^{-1} correspond to the stretching mode due to Cu–Cu dimer moieties and Cu–O, where 'O' corresponds to the oxygen from water adsorbed on Cu^{2+} ions. A minor peak at 450 cm^{-1} relates to the stretching modes of Cu–O related to the oxygen of the carboxylate bridges.

The bending vibration modes of C–H are observed at 742 cm^{-1} and 820 cm^{-1} respectively. The next peak observed around 1006 cm^{-1} is caused by the symmetric stretching mode of C=C moieties. The region from 1400 to 1600 cm^{-1} is attributed to the vibrational mode of carboxylate groups wherein the peak at 1547 cm^{-1} is due to the stretching asymmetric vibration of $C–O_2$ and 1458 cm^{-1} is due to the stretching symmetric vibrational frequency of $C–O_2$ along with bending vibration peak. Hence, results confirm the Meso-Cu-BTC formation in accordance with the literature report [49].

Thermogravimetric investigation was further done to understand the stability of the Meso-Cu-BTC framework and to cater the same, TGA analysis was done from room temperature to 800 °C under N_2 atmosphere (figure 6).

During the 1st stage, a weight loss of 19.2% was observed from 20 °C–100 °C, which is due to the lack of physically adsorbed H_2O molecules and organic solvents. This peak is well complemented with DSC results, wherein an endothermic peak (100 °C–290 °C) was seen as a result of dehydration of Meso-Cu-BTC molecules. A further second stage weight loss of 60% was observed from 200 °C–400 °C, which might be due to the loss of

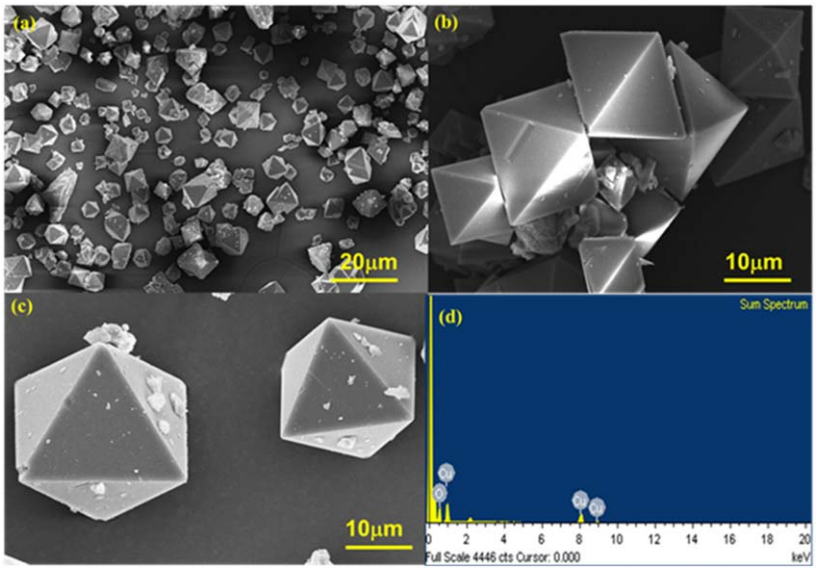

Figure 2. (a)–(c) FE-SEM images of Cu-BTC metal organic framework at different magnifications and (d) EDX.

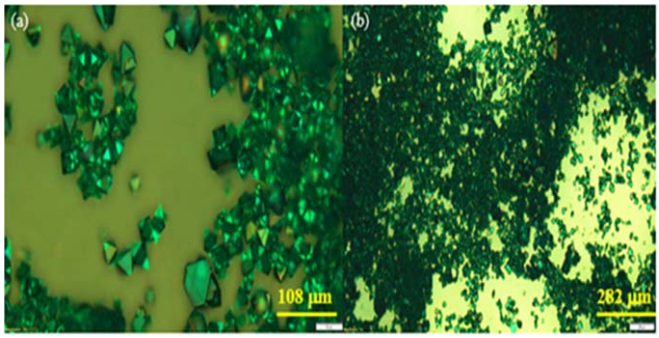

Figure 3. Optical microscopical images of Cu-BTC Metal organic framework at different magnifications.

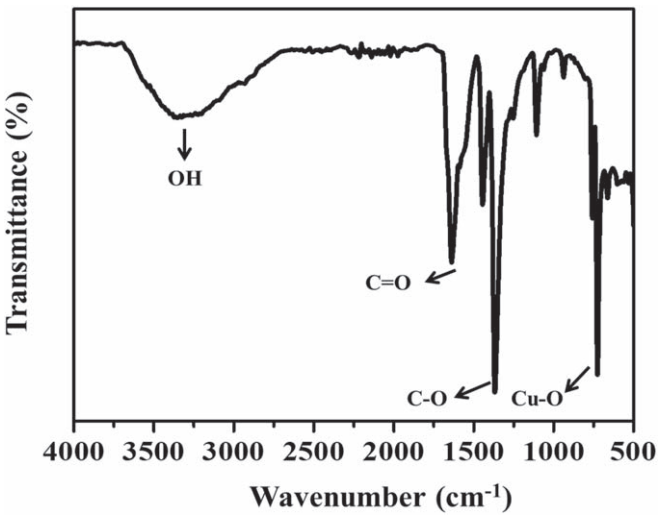

Figure 4. FTIR spectrum of Cu-BTC metal organic framework.

BTC ligand molecules and finally, a weight loss of 7.1% around 450 °C occurred due to the remaining linkers and decomposition of the sample with 26.5% remaining due to Cu metal and the degraded sample. In the DSC analysis, two exothermic peaks after 280 °C were observed, which are due to the formation of Cu_2O [50] and the

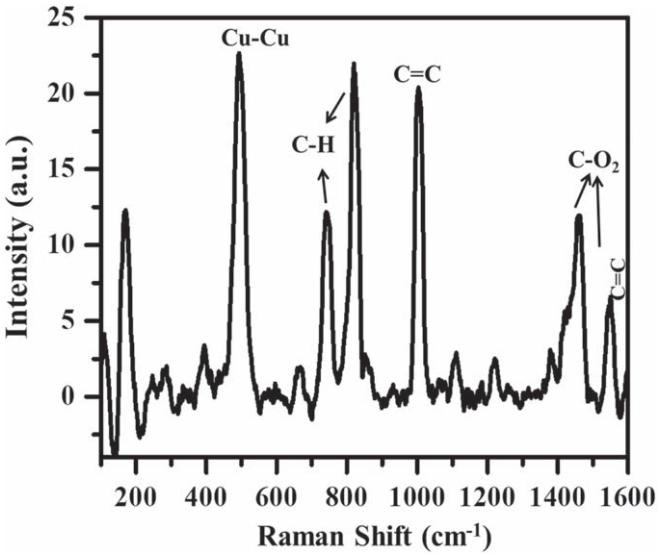

Figure 5. Raman spectrum of Cu-BTC metal organic framework.

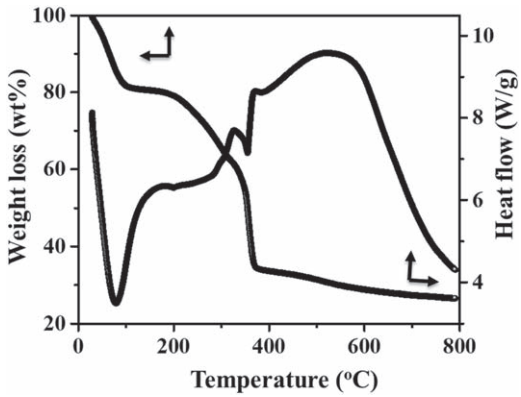

Figure 6. TGA/DSC curves of Cu-BTC Metal organic framework.

phase transformation of Cu_2O to CuO as per the earlier reports [51]. The theoretical weight loss percentage of water molecules is 16.2%, which is agreeable with the experimental weight loss around 17.2% due to the entire water molecules coordinated.

To further investigate the surface textural properties, N_2 adsorption-desorption of Meso-Cu-BTC MOF is taken and the corresponding result is given in figure 7. The synthesized catalyst exhibits a type IV IUPAC isotherm showing the presence of mesopores [52]. The surface area was calculated to be 540.2 $m^2\ g^{-1}$ by Brunauer–Emmett–Teller Model. Further to understand the pore structure, the pore size distribution of the catalyst was assessed from the adsorption curve isotherm by BJH method with an average diameter calculated to be 3.95 nm with a total pore volume calculated as 0.069 cc g^{-1}. Hence, these results indicate that the synthesized Meso-Cu-BTC catalyst have a high surface area, which could be a factor to enhance the electrocatalytic activity.

3.3. Hydrogen evolution reaction measurements

In view of investigating the electrocatalytic activity of Meso-Cu-BTC catalysts towards hydrogen evolution, the same was done using a standard three probe system (figures 8(a) and (b)) in alkaline medium [53]. LSV curves of the Meso-Cu-BTC electrocatalyst for hydrogen evolution reaction were recorded at 2 mVs^{-1} within a potential window of −0.4 to 0.4 V with reference to RHE electrode. The onset potential of Meso-Cu-BTC was observed to be 0.025 V and −0.002 V for Pt wire. Results show that Meso-Cu-BTC catalyst has proven to show fast electron capabilities towards HER. The good HER activity was further investigated by understanding the Tafel slopes of Cu-BTC electrode (figure 8(b)). To investigate the HER kinetics, overpotential versus log j was plotted (Tafel curve) and were further fitted into the linear portion of Tafel equation as follows

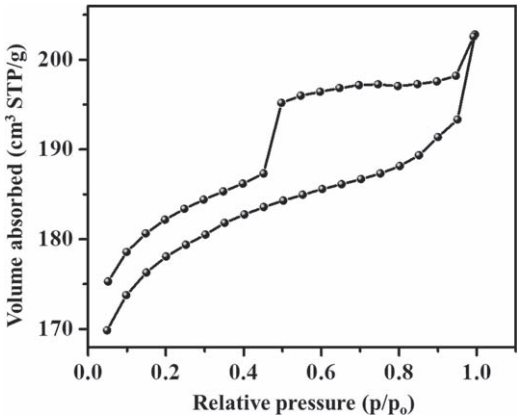

Figure 7. BET surface areas calculated from N_2 adsorption-desorption isotherms of Cu-BTC.

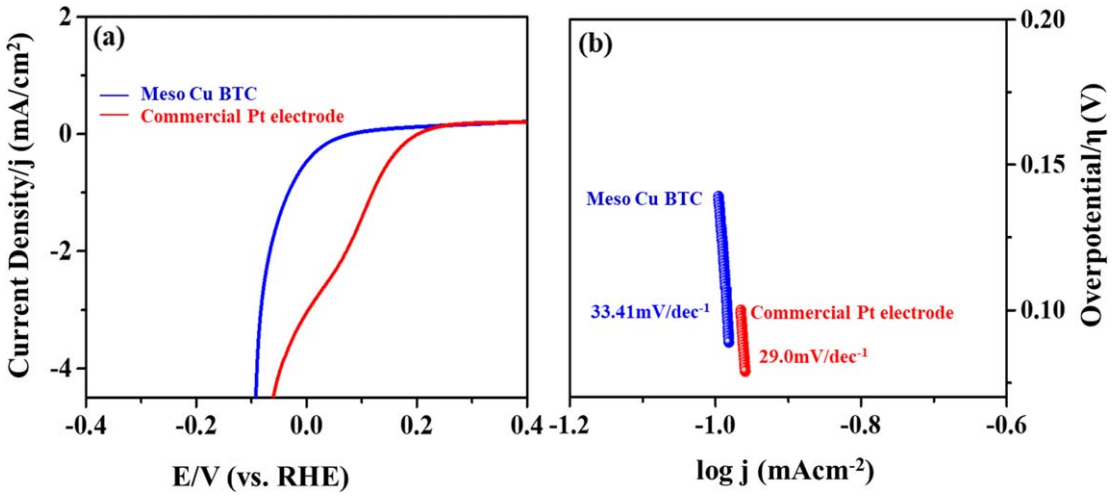

Figure 8. (a) LSV steady-state polarization plots of Meso CuBTC and Pt electrode and (b) Tafel plot for Meso Cu-BTC and Pt electrode in 1 M NaOH.

$$\eta = a + b \log j$$

where j is the current density, η is the overpotential; b represents the Tafel slope (figure 8(b)). A small Tafel slope value represents the excellent activity as a low overpotential is needed to reach the equal current density.

Tafel slope value of Meso-Cu-BTC and Pt electrode, 33.41 and 29.0 $mVdec^{-1}$. Besides, another important factor in HER is the exchange current density (j_o), the same could be estimated by extrapolating the Tafel plot. It is found that Meso-Cu-BTC exhibited a j_o of 6 $mAcm^{-2}$ with overpotential of 89.32 mV, whereas for conventional Pt, it was found to be 6.8 $mAcm^{-2}$ with overpotential of 79.0 mV. As observed from the results, it is clear that Meso-Cu-BTC exhibited near slope as Pt, which means faster reaction kinetics as conventional Pt. In the Tafel plot, three reaction steps are observed in alkaline medium, a primary discharge step (Volmer mechanism with Tafel slope of 120 $mVdec^{-1}$) - the cathodic reaction of proton, which produced H^+ ions to generate the hydrogen molecules and Heyrovsky mechanism with 40 $mVdec^{-1}$ Tafel slope as the second step of electrochemical desorption or discharge reaction of H and H^+ from the surface of the catalyst to form hydrogen and Tafel reaction mechanism with a Tafel slope ~30 $mVdec^{-1}$ is the last step to produce hydrogen [50, 54, 55].

$$H_2O + M + e^- \rightarrow M - H_{ads} + OH^-(\text{Volmer})$$

$$H_2O + M - H_{ads} + e^- \rightarrow H_2 + M + OH^- \text{ (Heyrovsky)}$$

$$2M - H_{ads} \rightarrow 2M + H_2(\text{Tafel})$$

where MH_{ads} is the absorbed H_2 atom over the metal surface and M is the active free catalytic sites available for HER. In the case of Tafel plots, a slope of 33.41 $mVdec^{-1}$, 29.0 $mVdec^{-1}$ was observed, which is lower than 40 $mVdec^{-1}$ indicating a Tafel controlled reaction. Thus, based on the slope obtained, it clear that the HER reaction mechanism is controlled by Tafel mechanism. The observed results given in table 1 show that Cu-BTC catalyst is comparable to Pt electrode proving to be a good electrocatalyst for HER. An overall table of

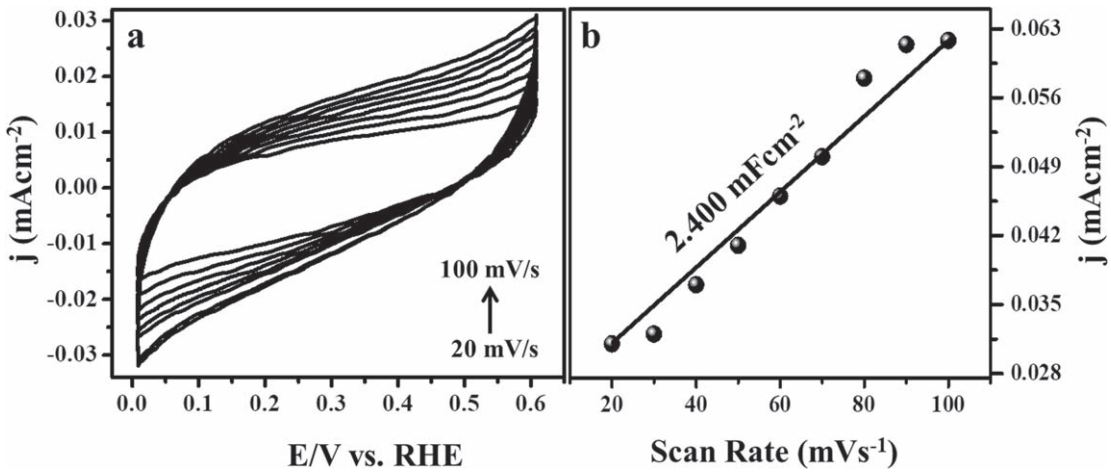

Figure 9. (a) Cyclic voltammetry analysis of Cu-BTC at various scan rates (b) the corresponding capacitive current densities as a function of scan rate.

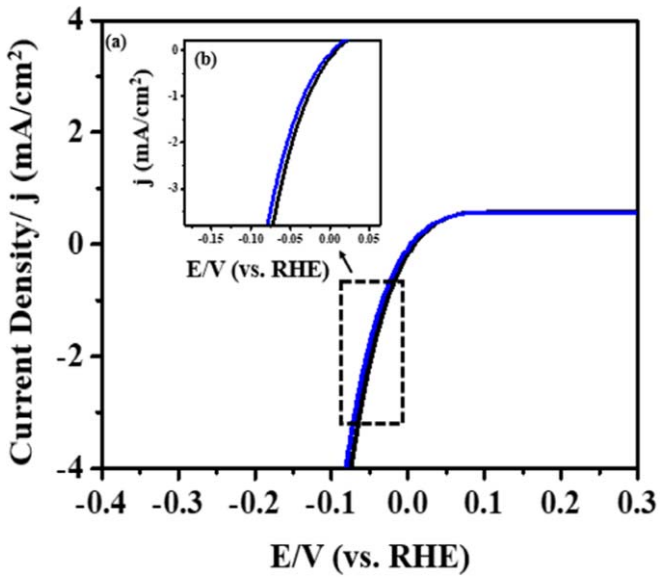

Figure 10. Polarization curves for Cu-BTC electrode for initial and after 1000 cycles in 1 M NaOH.

comparison is given in table S1, which shows that the prepared Meso-Cu-BTC catalyst exhibits excellent activity than the reported one.

Long term durability test is an important parameter for HER catalyst and in this regard, polarization was carried out for 1000 cycles. The prepared Meso-Cu-BTC catalyst was tested for its stability over 1000 cycles from −0.4 to 0.4 V at 2 mV s^{-1} scan rate and the same is given in figure 10. The polarization curves show that no significant decay was observed even after 1000 cycles indicating that Meso-Cu-BTC catalyst has excellent stability and durability towards HER. The electrochemical active surface area of Meso-Cu-BTC electrode gives the surface area accessible and the same could be calculated by the double-layer capacitance (Cdl) using the cyclic voltammetric technique. ECSA was estimated by CV curves at various scan rates (100–20 mV s^{-1}) in the non-faradic region and the double layer capacitance was calculated as per the Mccory's theory (figure 9(a) and 9(b)). As per the theory, the EDLC calculated from the capacitive current at different scan rates serves as an assessment of the active electrochemical active surface area of the solid-liquid interface [56]. The cyclic voltammetry was run between a region of 0 to 0.6 V, where the characteristic Faradic process was seen. The measured Cdl value from 20–100 mV s^{-1} scan rate is given figure 9(b) and from the graphs, Cdl was calculated to be 2.4 mF cm^{-2}, which shows that Meso-Cu-BTC are electrochemically active in alkaline medium. Moreover, high active surface area and electrical conductivity of Meso-Cu-BTC suggest the high electrochemical activity for HER.

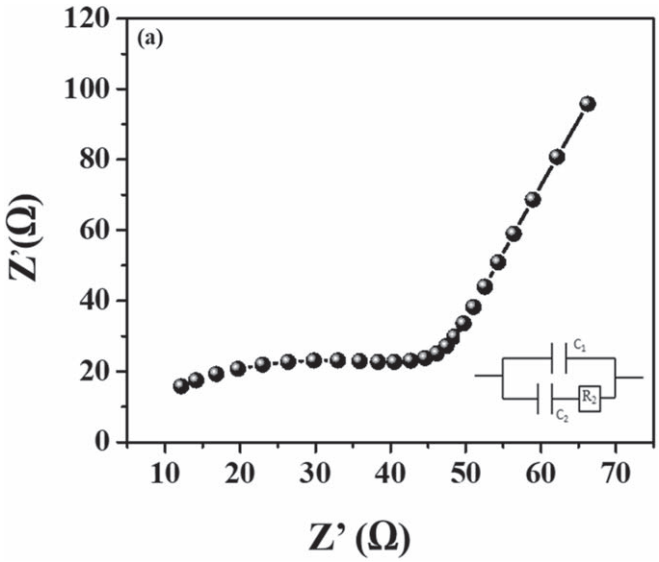

Figure 11. Nyquist plot for Cu-BTC in 1 M NaOH recorded at 200 mV versus RHE.

Table 1. Tafel slope and Exchange current densities of HER using Meso-Cu-BTC Metal organic framework.

S. no	Catalyst	$\log j_o$mA cm^{-2}	bmV dec^{-1}	α
1	Pt Electrode	6.8	29.0	2.05
2	CuBTC	6.0	33.41	1.78

To further understand the nature of the catalytic process and to reveal the interfacial interaction and kinetics of Meso-Cu-BTC electrode, electrochemical impedance spectroscopy (EIS) was done (figure 11). The diameter of the semicircle at the high-frequency range is due to the porous nature of the electrode surface whereas the line with potential dependent properties at low frequencies is associated with the HER kinetics [57]. In the electrochemical reaction process at the surface of the electrode, catalytic kinetics was determined by Rct, wherein a smaller Rct value shows faster kinetics. The Rct value for Meso-Cu-BTC electrode was found to 15.8 ohm. This lower charge transfer resistance Rct value enhances the electrochemical properties towards hydrogen evolution reaction, owing to its high conductivity surface and well hydrogen adsorption capacity [58]. Hence, results conclude that Meso-Cu-BTC catalyst has a lower resistance due to the fast electron transport rate between the interface and exhibiting an excellent hydrogen evolution reaction activity in alkaline medium.

4. Conclusion

In conclusion, a simple and facile solvothermal route was used for the synthesis of Meso-Cu-BTC MOFsl and further used for the efficient electrocatalysis of HER in alkaline medium. The Meso-Cu-BTC electrocatalyst exhibited 25 mV onset potential, 89.32 mV overpotential, 33.41 mVdec^{-1} Tafel slope value, 6.0 mA cm^{-2} exchange current density and no significant decay even after 1000 cycles. Further, the Tafel slope for Meso-Cu-BTC catalyst suggests the recombination step in the electrocatalysis of HER. These results are mainly associated with a highly porous network of Meso-Cu-BTC octahedral MOF for fast electronic and ionic transfer from the surface of the electrocatalyst particles. This work paves the way for the development of low-cost electrocatalyst for HER with high efficiency and stability.

ORCID iDs

George Jacob https://orcid.org/0000-0001-8311-6700
Vimala Raghavan https://orcid.org/0000-0002-3697-9041
Krishna Chandar N https://orcid.org/0000-0001-9759-5714
Andrews Nirmala Grace https://orcid.org/0000-0002-8714-1716

References

[1] Dresselhaus M S and Thomas I L 2001 Alternative energy technologies *Nature* **414** 332–7
[2] Lewis N S 2007 Toward cost-effective solar energy use *Science* **315** 798–801
[3] Turner J A 2004 Sustainable hydrogen production *Science* **305** 972–4
[4] Hoffert M I *et al* 2002 Advanced technology paths to global climate stability: energy for a greenhouse planet *Science* **298** 981–7
[5] Gómez M J, Loiácono A, Pérez L A, Franceschini E A and Lacconi G I 2019 Highly efficient hybrid Ni/nitrogenated graphene electrocatalysts for hydrogen evolution reaction *ACS Omega.* **4** 2206–16
[6] Muthurasu A, Maruthapandian V and Kim H Y 2019 Metal-organic framework derived Co_3O_4/MoS_2 heterostructure for efficient bifunctional electrocatalysts for oxygen evolution reaction and hydrogen evolution reaction *Appl. Catalysis* B **248** 202–10
[7] Lim K L, Kazemian H, Yaakob Z and Daud W R 2010 Solid-state materials and methods for hydrogen storage: a critical review *Chemical Engineering & Technology: Industrial Chemistry-Plant Equipment-Process Engineering-Biotechnology* **33** 213–26
[8] Iqbal S, Ali B, Shoaib A, Muhammad S, Guocong L, Li H, Muhammad R, Mohsin J and Bilal K 2020 Design novel morphologies of L-cysteine surface capped 2D covellite (CuS) nanoplates and study the effect of CuS morphologies on dye degradation rate under visible light *CrystEngComm* **22** 4162–73
[9] Shoaib A, Muwei J, Hongmei Q, Jiajia L, Meng X and Jiatao Z 2019 Noble metal nanoclusters and their *in situ* calcination to nanocrystals: precise control of their size and interface with TiO_2 nanosheets and their versatile catalysis applications *Nano Res.* **9** 1763–74
[10] Xu T, Wei S, Zhang X, Zhang D, Xu Y and Cui X 2019 Sulfur-doped Cu3P| S electrocatalyst for hydrogen evolution reaction *Mater. Res. Express* **6** 075501
[11] Wu C, Li C, Yang B, Zhou S, Shi D, Wang Y, Yang G, He J and Shan Y 2016 Electrospun $MnCo_2O_4$ nanofibers for efficient hydrogen evolution reaction *Mater. Res. Express* **3** 095018
[12] Zhao X, Fan Y, Wang H, Gao C, Liu Z, Li B, Peng Z, Yang J-H and Liu B 2020 Cobalt phosphide-embedded reduced graphene oxide as a bifunctional catalyst for overall water splitting *ACS Omega* **12** 6516–22
[13] Iqbal S, Ali B, Shoaib A, Shahid A, Aamer S, Rana M I, Li H, Mohsin J, Muhammad R and Muhammad S 2020 Shape and phase-controlled synthesis of specially designed 2D morphologies of L-cysteine surface capped covellite (CuS) and chalcocite (Cu_2S) with excellent photocatalytic properties in the visible spectrum *Appl. Surf. Sci.* **526** 146691
[14] Ghosh S and Basu R N 2018 Multifunctional nanostructured electrocatalysts for energy conversion and storage: current status and perspectives *Nanoscale.* **10** 11241–80
[15] Voiry D, Salehi M, Silva R, Fujita T, Chen M, Asefa T, Shenoy V B, Eda G and Chhowalla M 2013 Conducting MoS_2 nanosheets as catalysts for hydrogen evolution reaction *Nano Lett.* **13** 6222–7
[16] Lihong T, Yan X and Chen X 2016 *ACS Catal.* **6** 5441–8
[17] Wan C, Regmi Y N and Leonard B M 2014 Multiple phases of molybdenum carbide as electrocatalysts for the hydrogen evolution reaction *Angew. Chem. Int. Ed.* **53** 6407–10
[18] Bradshaw D, Garai A and Huo J 2012 Metal–organic framework growth at functional interfaces: thin films and composites for diverse applications *Chem. Soc. Rev.* **41** 2344–81
[19] Khan M A, Mutahir S, Wang F, Lei W and Xia M 2018 Sensitization of TiO_2 nanosheets with Cu–biphenylamine framework to enhance photocatalytic degradation performance of toxic organic contaminants: synthesis, mechanism and kinetic studies *Nanotechnology* **29** 375605
[20] Cui Y, Yue Y, Qian G and Chen B 2012 Luminescent functional metal–organic frameworks *Chem. Rev.* **112** 1126–62
[21] Crawford S E, Kim K J, Yu Y and Ohodnicki P R 2018 Rapid, selective, ambient growth and optimization of copper benzene-1, 3, 5-tricarboxylate (Cu–BTC) metal–organic framework thin films on a conductive metal oxide *Crystal Growth & Design* **18** 2924–31
[22] Humphrey S M, Angliss T J, Aransay M, Cave D, Gerrard L A, Weldon G F and Wood P T 2007 Bimetallic metal-organic frameworks containing the $M(2,x-pdc)_2^{2-}$ (M = Cu, Pd, Pt; x = 4, 5) building block–synthesis, structure, and magnetic properties *Z. Anorg. Allg. Chem.* **633** 2342–53
[23] Zhang X M, Hao Z M, Zhang W X and Chen X M 2007 Dehydration-induced conversion from a single-chain magnet into a metamagnet in a homometallic nanoporous metal–organic framework *Angew. Chem. Int. Ed.* **46** 3456–9
[24] Maspoch D, Ruiz-Molina D and Veciana J 2004 Magnetic nanoporous coordination polymers *J. Mater. Chem.* **14** 2713–23
[25] Du D Y, Qin J S, Li S L, Su Z M and Lan Y Q 2014 Recent advances in porous polyoxometalate-based metal–organic framework materials *Chem. Soc. Rev.* **43** 4615–32
[26] Clough A J, Yoo J W, Mecklenburg M H and Marinescu S C 2015 Two-dimensional metal–organic surfaces for efficient hydrogen evolution from water *JACS* **137** 118–21
[27] Chui S S, Lo S M, Charmant J P, Orpen A G and Williams I D 1999 A chemically functionalizable nanoporous material $[Cu_3(TMA)_2(H_2O)_3]$ n *Science* **283** 1148–50
[28] C Chen B, Ockwig N W, Millward A R, Contreras D S and Yaghi O M 2005 High H_2 adsorption in a microporous metal–organic framework with open metal sites *Angew. Chem. Int. Ed.* **44** 4745–9
[29] Yang Q and Zhong C 2006 Understanding hydrogen adsorption in metal− organic frameworks with open metal sites: a computational study *J. Phys. Chem.* B **110** 655–8
[30] Abbasi A R, Karimi M and Daasbjerg K 2017 Efficient removal of crystal violet and methylene blue from wastewater by ultrasound nanoparticles Cu-MOF in comparison with mechanosynthesis method *Ultrason. Sonochem.* **37** 182–91
[31] Wei B, Wu J, Mei G, Qi Z, Hu W and Wang Z 2019 $NiCo_2O_4$ nanowire arrays rich in oxygen deficiencies for hydrogen evolution reaction *Int. J. Hydrogen Energy* **44** 6612–7
[32] Roy A, Hursán D, Artyushkova K, Atanassov P, Janáky C and Serov A 2018 Nanostructured metal-NC electrocatalysts for CO_2 reduction and hydrogen evolution reactions *Appl. Catalysis* B **232** 512–20
[33] Song J, Gu X, Cheng J, Fan N, Zhang H and Su H 2018 Remarkably boosting catalytic H_2 evolution from ammonia borane through the visible-light-driven synergistic electron effect of non-plasmonic noble-metal-free nanoparticles and photoactive metal-organic frameworks *Appl. Catalysis* B **225** 424–32
[34] Pillai S B, Dabhi S D and Jha P K 2018 Hydrogen evolution reaction and electronic structure calculation of two dimensional bismuth and its alloys *Int. J. Hydrogen Energy* **43** 21649–54
[35] Raoof J B, Hosseini S R, Ojani R and Mandegarzad S 2015 MOF-derived Cu/nanoporous carbon composite and its application for electro-catalysis of hydrogen evolution reaction *Energy* **90** 1075–81
[36] Hong W, Jian C, Wang G, He X, Li J, Cai Q, Wen Z and Liu W 2019 Self-supported nanoporous cobalt phosphosulfate electrodes for efficient hydrogen evolution reaction *Appl. Catalysis* B **251** 213–9

[37] Song T, Zhang L, Zhang P, Zeng J, Wang T, Ali A and Zeng H 2017 Stable and improved visible-light photocatalytic hydrogen evolution using copper (ii)–organic frameworks: engineering the crystal structures *J. Mater. Chem.* A **5** 6013–8
[38] Xu W, Li G, Li W and Zhang H 2016 Facile room temperature synthesis of metal–organic frameworks from newly synthesized copper/zinc hydroxide and their application in adsorptive desulfurization *RSC Adv.* **6** 37530–4
[39] S Lin S, Song Z, Che G, Ren A, Li P, Liu C and Zhang J 2014 Adsorption behavior of metal–organic frameworks for methylene blue from aqueous solution *Microporous Mesoporous Mater.* **193** 27–34
[40] Benck J D, Hellstern T R, Kibsgaard J, Chakthranont P and Jaramillo T F 2014 Catalyzing the hydrogen evolution reaction (HER) with molybdenum sulfide nanomaterials *ACS Catal.* **4** 3957–71
[41] Alfè M, Gargiulo V, Lisi L and Di Capua R 2014 Synthesis and characterization of conductive copper-based metal-organic framework/graphene-like composites *Mater. Chem. Phys.* **147** 744–50
[42] Yang Y, Shukla P, Wang S, Rudolph V, Chen X M and Zhu Z 2013 Significant improvement of surface area and CO_2 adsorption of Cu–BTC via solvent exchange activation *RSC Adv.* **3** 17065–72
[43] Kim K J, Li Y J, Kreider P B, Chang C H, Wannenmacher N, Thallapally P K and Ahn H G 2013 High-rate synthesis of Cu–BTC metal–organic frameworks *Chem. Commun.* **49** 11518–20
[44] IUPAC 1972 *Manual of Symbols and Terminology for Physicochemical Quantities and Units* (London: Butterworths)
[45] Sánchez M, Rams J and Urena A 2008 Oxidation mechanisms of copper and nickel coated carbon fibers *Oxid. Met.* **69** 327–41
[46] Ganesan R and Lee J S 2006 An electrocatalyst for methanol oxidation based on tungsten trioxide microspheres and platinum *J. Power Sources* **157** 217–21
[47] Kaninski M P, Nikolić V M, Potkonjak T N, Simonović B R and Potkonjak N I 2007 Catalytic activity of Pt-based intermetallics for the hydrogen production—influence of ionic activator *Appl. Catal.* A **321** 93–9
[48] Al Cheikh J, Villagra A, Ranjbari A, Pradon A, Antuch M, Dragoe D, Millet P and Assaud L 2019 Engineering a cobalt clathrochelate/glassy carbon interface for the hydrogen evolution reaction *Appl. Catalysis* B **250** 292–300
[49] Feng L L, Fan M, Wu Y, Liu Y, Li G D, Chen H, Chen W, Wang D and Zou X 2016 Metallic Co9S8 nanosheets grown on carbon cloth as efficient binder-free electrocatalysts for the hydrogen evolution reaction in neutral media *J. Mater. Chem.* A **4** 6860–7
[50] Huang J F and Wu Y C 2018 Making Ag present Pt-like activity for hydrogen evolution reaction *ACS Sustainable Chemistry & Engineering* **6** 8285–90
[51] Czerw R *et al* 2001 Identification of electron donor states in N-doped carbon nanotubes *Nano Lett.* **1** 457–60
[52] Qu Y, Shao M, Shao Y, Yang M, Xu J, Kwok C T, Shi X, Lu Z and Pan H 2017 Ultra-high electrocatalytic activity of VS2 nanoflowers for efficient hydrogen evolution reaction *J. Mater. Chem.* A **5** 15080–6
[53] Du K, Zheng L, Wang T, Zhuo J, Zhu Z, Shao Y and Li M 2017 Electrodeposited Mo3S13 films from (NH4) 2Mo3S13 · 2H2O for electrocatalysis of hydrogen evolution reaction *ACS Applied Materials & Interfaces* **9** 18675–81
[54] Ma L, Shen X, Zhou H, Zhu G, Ji Z and Chen K 2015 CoP nanoparticles deposited on reduced graphene oxide sheets as an active electrocatalyst for the hydrogen evolution reaction *J. Mater. Chem.* A **3** 5337–43
[55] Niu J, Domenech-Carbó A, Primo A and Garcia H 2019 Uniform nanoporous graphene sponge from natural polysaccharides as a metal-free electrocatalyst for hydrogen generation *RSC Adv.* **9** 99–106
[56] Wu Y P, Zhou W, Zhao J, Dong W W, Lan Y Q, Li D S, Sun C and Bu X 2017 Surfactant-assisted phase-selective synthesis of new cobalt MOFs and their efficient electrocatalytic hydrogen evolution reaction *Angew. Chem. Int. Ed.* **56** 13001–5
[57] Hod I *et al* 2015 A porous proton-relaying metal-organic framework material that accelerates electrochemical hydrogen evolution *Nat. Commun.* **6** 1–9
[58] Chowdhury P, Mekala S, Dreisbach F and Gumma S 2012 Adsorption of CO, CO_2 and CH_4 on Cu-BTC and MIL-101 metal organic frameworks: effect of open metal sites and adsorbate polarity *Microporous Mesoporous Mater.* **152** 246–52